the tube, and the tube disengagement process.

(3) The dipole moment per unit contour length of *cis*-PI is 3.31×10^{-12} to 4.80×10^{-12} cgs esu depending on the assumption of the internal field. The perpendicular dipole component per the repeat unit was determined to be 0.21 D.

Acknowledgment. We thank Professor Masao Doi of Tokyo Metropolitan University for helpful discussion. We also thank Dr. Kazuyuki Tatsumi of Osaka University, who kindly made the computer calculation of the dipole moment of *cis*-Polyisoprene. This work was supported partly by the Institute of Polymer Research, Osaka University.

Registry No. Polyisoprene (homopolymer), 9003-31-0.

References and Notes

(1) Stockmayer, W. H. *Pure Appl. Chem.* **1967**, *15*, 539.
(2) North, A. M. *Chem. Soc. Rev.* **1972**, *1*, 49.
(3) Adachi, K.; Kotaka, T. *Macromolecules* **1983**, *16*, 1936.
(4) Rouse, P. E. *J. Chem. Phys.* **1953**, *21*, 1272.
(5) Zimm, B. H. *J. Chem. Phys.* **1956**, *24*, 269.
(6) Adachi, K.; Kotaka, T. *Macromolecules* **1984**, *17*, 120.
(7) Stockmayer, W. H.; Baur, M. E. *J. Am. Chem. Soc.* **1964**, *86*, 3485.
(8) Baur, M. E.; Stockmayer, W. H. *J. Chem. Phys.* **1965**, *43*, 4319.
(9) Stockmayer, W. H.; Burke, J. J. *Macromolecules* **1969**, *2*, 647.
(10) Jones, A. A.; Stockmayer, W. H.; Molinari, R. J. *J. Polym. Sci., Polym. Symp.* **1976**, *No. 54*, 227.
(11) North, A. M.; Phillips, P. J. *Trans. Faraday Soc.* **1968**, *64*, 3235.
(12) Hirose, M.; Yamakawa, N.; Araki, K.; Imamura, Y. *Rep. Prog. Polym. Phys. Jpn.* **1976**, *20*, 117.
(13) Ferry, J. D. "Viscoelastic Properties of Polymers"; Wiley: New York, 1961.
(14) Graessley, W. W. *Adv. Polym. Sci.* **1974**, *16*, 1.
(15) de Gennes, P.-G. *J. Chem. Phys.* **1971**, *55*, 572.
(16) de Gennes, P.-G. "Scaling Concepts in Polymer Physics"; Cornell University Press: Ithaca, NY, 1979.
(17) Doi, M.; Edwards, S. F. *J. Chem. Soc., Faraday Trans. 2* **1978**, *74*, 1789, 1802, 1818.
(18) McCrum, N. G.; Read, B. E.; Williams, G. "Anelastic and Dielectric Effects in Polymeric Solids"; Wiley: New York, 1967.
(19) Morton, M.; Fetters, L. J. *Rubber Chem. Technol.* **1975**, *48*, 359.
(20) Adachi, K.; Hirose, Y.; Ishida, Y. *J. Polym. Sci., Polym. Phys. Ed.* **1975**, *13*, 1491.
(21) Vogel, H. *Z. Phys.* **1921**, *22*, 645.
(22) Tamman, G.; Hesse, W. *Z. Anorg. Allg. Chem.* **1926**, *156*, 245.
(23) Nemoto, N.; Moriwaki, M.; Odani, H.; Kurata, M. *Macromolecules* **1971**, *4*, 215.
(24) Nemoto, N.; Odani, H.; Kurata, M. *Macromolecules* **1972**, *5*, 531.
(25) Havriliak, S.; Negami, S. *J. Polym. Sci., Part. C* **1966**, *No. 14*, 99.
(26) Flory, P. J.; Fox, T. G. *J. Am. Chem. Soc.* **1951**, *73*, 1907, 1909, 1915.
(27) Poddubnyi, I. Y.; Ehrenberg, E. G. *J. Polym. Sci.* **1962**, *57*, 545.
(28) Le Fevre, R. J. W. "Dipole Moment"; Wiley: New York, 1964.
(29) Adachi, K.; Okazaki, H.; Kotaka, T., unpublished data.
(30) Mark, J. E. *J. Am. Chem. Soc.* **1966**, *88*, 4354.
(31) Smyth, C. P. *J. Am. Chem. Soc.* **1929**, *51*, 2380.
(32) Tatsumi, K., unpublished data.
(33) Berry, G. C.; Fox T. G. *Adv. Polym. Sci.* **1969**, *6*, 1.
(34) Doi, M. *J. Polym. Sci., Polym. Phys. Ed.* **1983**, *21*, 667.
(35) Cole, R. H. *J. Chem. Phys.* **1975**, *42*, 637.
(36) Doi, M., private communication.
(37) van Krevelen, D. W. "Properties of Polymers", 2nd ed.; Elsevier: Amsterdam, 1976.

Oriented Crystallization of Cross-Linked Polybutadiene Rubber. 2. Small-Angle and Wide-Angle X-ray Scattering

Takeji Hashimoto,* Kenji Saijo, Michał Kość,† and Hiromichi Kawai

Department of Polymer Chemistry, Faculty of Engineering, Kyoto University, Sakyo-ku, Kyoto 606, Japan

Andrzej Wasiak and Anderzej Ziabicki

Polish Academy of Sciences, Institute of Fundamental Technological Research, 00-049 Warszawa, Poland. *Received November 14, 1983*

ABSTRACT: Effects of amorphous chain orientation on the orientation distribution of crystallites formed by oriented crystallization of cross-linked *cis*-1,4-polybutadiene were investigated by using small-angle (SAXS) and wide-angle X-ray scattering (WAXS). Orientation distribution of lamellar normals $q_l(\psi)$ and of the reciprocal lattice vectors, $q_{hkl}(\psi)$ of the (110) and (020) planes, were presented as functions of crystallization temperature (T_c = 240–260 K) and draw ratios (λ = 1.6–3.0). The results indicate that the higher the temperature T_c and the larger the draw ratio λ, the sharper are the orientation distributions $q_l(\psi)$ and $q_{hkl}(\psi)$ produced. It has been shown that the observed phenomena can be understood on the basis of either of the two asymptotic crystallization theories: (i) equilibrium theory of crystallization in a phantom network and (ii) kinetic theory of nucleation in a system of asymmetric elements.

I. Introduction

Oriented crystallization of cross-linked polymers has been of interest to theoreticians and experimentalists since the beginning of polymer science. It involves a fundamental problem concerning the effect of molecular orientation (i.e., a reduction of conformational entropy of long-chain molecules) on phase transition. The fundamental molecular theories of oriented crystallization include the theory of Flory,[1] developed later by Smith[2] and Wu,[3] theories of Krigbaum and Roe,[4] Gaylord,[5] Baranov and Elyashevich,[6] Jarecki and Ziabicki,[7,36] and Allegra.[8] Experimental aspects of the problem have been investigated by Gehman and Field,[9] Kawai,[10] Keller,[11] Luch and Yeh,[12] Cesari,[13] and others.[14-20]

The aim of this work was to study crystallite orientation in isothermally crystallized cross-linked *cis*-1,4-polybutadiene in the stretched state and to explain its nature on the basis of equilibrium and kinetic theories. Crystallite orientation in polymers crystallized under molecular ori-

† On leave from the Polish Academy of Sciences.

0024-9297/85/2218-0472$01.50/0

entation has not been fully analyzed. Most experimental studies[9-11,13] have been confined to qualitative analyses and did not attempt comparison of the experimental results with theoretical predictions. Theoretical approaches to the problem of crystallite orientation at the molecular level were also qualitative and often oversimplified. In many papers it is assumed that crystallites are perfectly oriented along the stretching direction.[1-3] An exception is the treatment of Allegra,[8] who presented a theory of orientation-dependent crystallization and interpreted experimental data obtained by Cesari.[13] Our study involves crystallization conditions different from those of Allegra and Cesari: temperatures below the melting temperature of an unstressed polymer. Our theoretical treatment is also different, being based on the theory of equilibrium crystallization in polymer networks[21] and the kinetic theory of nucleation.[31-33]

We have studied crystallite orientation by quantitatively measuring normalized orientation distribution functions of crystallographic axes (reciprocal lattice vectors (110) and (020), or c axis) or lamellae normals under various crystallization conditions. The normalized orientation distribution functions of reciprocal lattice vectors and their second moments were determined by quantitative wide-angle X-ray diffraction (WAXS). The corresponding distribution function for the lamellar normal and its second moment were determined by quantitative small-angle X-ray scattering (SAXS) with a point-collimating system. Point collimation was employed to avoid complication of the analysis by anisotropic slit-smearing effects[40] and was chosen so that its weighting function was much narrower than those of the SAXS profiles. Such SAXS measurements have recently become possible owing to developments of strong X-ray sources and position-sensitive detectors.

II. Experimental Section

1. **Material.** The cross-linked polybutadiene samples were kindly supplied by Assoreni, San Donato Milanese (Italy). Polybutadiene (PB) was polymerized with uranium catalyst, yielding 99% cis 1,4-linkages, number-average molecular weight 1.2×10^5 in the un-cross-linked state, and corresponding to the sample coded "Uranium C" in the paper by Chirico et al.[22] The polymers were cross-linked by using Sulfasan R (4,4′-dithiomorpholine).[23,24] The cross-linked polybutadiene had a cross-link density 1×10^{-4} mol/cm^3 and a number-average molecular weight between cross-links of 9000.[23]

2. **Apparatus and Methods.** The orientation distribution of crystallites crystallized under constant draw ratio, λ, at constant crystallization temperature, T_c, was measured by WAXS and SAXS. The samples were uniaxially stretched at room temperature and clamped to the sample holder at given draw ratios, which were low enough to prevent crystallization at room temperature. The sample holder was then transferred into a metal block whose temperature was maintained at a given T_c. The samples were allowed to crystallize isothermally for periods of time long compared to the crystallization half-time $t_{1/2}$ as observed by SAXS and WAXS at given T_c and λ.[25] The stretching devices, the temperature enclosures, and the SAXS and WAXS systems will be described elsewhere.[26]

The SAXS and WAXS intensity distributions of the crystallized samples were measured as functions of scattering angle 2θ or s

$$s = (2 \sin \theta)/\lambda_w \qquad (\lambda_w\text{: X-ray wavelength}) \qquad \text{(II-1)}$$

and azimuthal angle (see Figure 1 for SAXS optics). The reduction of the scattered intensity involved in the point-collimating optics was partially compensated by using a high-flux X-ray source (12-kW rotating anode generator, RU-a, manufactured by Rigaku Denki) and a linear position-sensitive X-ray detector (PSPC) of the multiwired delay line type, also manufactured by Rigaku Denki.[27,28] Monochromatized Cu Kα radiation was used. The angular dependence of the scattered intensity $I(\psi)$ was measured by changing the stretching direction (SD) of the specimen while keeping the orientation of the linear detector horizontal. The angle ψ was defined as the angle between the SD and the horizontal direction of the apparatus (Figure 1).

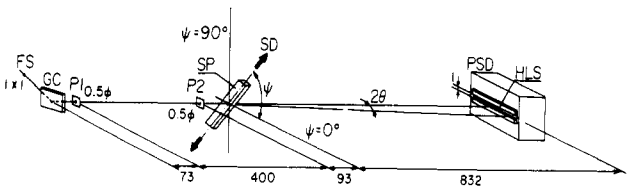

Figure 1. Schematic diagram for SAXS optics and definitions of the azimuthal (ψ) and scattering (2θ) angles: (FS) focal spot; (GC) graphite crystal; (P1 and P2) collimating pinholes; (SD) stretching direction; (HLS) height-limiting slit; (PSD) linear position-sensitive proportional counter.

III. Theoretical Background for Determining Orientation Distribution Functions of Lamellar Normals from SAXS Intensity Distributions

The quantitative determination of orientation distributions from SAXS has not been reported, although the azimuthal SAXS intensity distribution has often been used to discuss qualitatively the degree of orientation of lamellar normals with respect to a reference axis. The basic principle is the same as that of WAXS determination of the orientation distribution of reciprocal lattice vectors.[29,30,39]

We measured the intensity distribution of the SAXS pattern with s and ψ_1 (Figure 3a). In order to avoid complications due to slit-smearing effects,[40] we used the point-collimating system shown in Figure 1, in which a height-limiting slit (HLS) of width 1 mm generated nearly circularly symmetric slit weighting functions $W(u_1,u_2)$ having the same breadths along the slit-width (u_1) and slit-length (u_2) directions (see Figure 2).[27,28] The breadths of the weighting functions should ideally be much smaller than the breadths of the observed scattering intensity distribution $I(X,Y)$ (X and Y being the scattering angles along u_1 and u_2, respectively, i.e., in Figure 3 along horizontal and vertical directions, respectively). The observed distribution $\tilde{I}(X,Y)$ is related to the true scattering intensity distribution $I(X,Y)$ by

$$\tilde{I}(X,Y) = \int\int du_1\, du_2\, W(u_1,u_2) I(X-u_1, Y-u_2) \qquad \text{(III-1)}$$

If the distributions of $W(X,Y)$ with X and Y are much narrower than those of $I(X,Y)$ with X and Y, then

$$I(X,Y) \simeq \int\int du_1\, du_2\, \delta(u_1,u_2) I(X-u_1, Y-u_2) \qquad \text{(III-2)}$$

$$= I(X,Y) \qquad \text{(III-3)}$$

where $\delta(u_1,u_2)$ is a δ function. In this case the measured SAXS intensity distribution $\tilde{I}$ is free from the smearing effect and is equal to the true scattered intensity distribution $I(X,Y)$.

The optical system shown in Figure 1 satisfies the above criterion, and the weighting function $W(u_1,u_2)$ was measured by a method described elsewhere.[27,28] It was shown also that $W(u_1,u_2)$ can be given by

$$W(u_1,u_2) = W_W(u_1) W_H(u_2) \qquad \text{(III-4)}$$

where measured functions $W_W(u_1)$ and $W_H(u_2)$ are presented in Figure 2. The slit-width (W_W) and slit-height weighting functions (W_H) are identical, assuring a point-collimating system. The full width at half-maximum (fwhm) of the weighting functions W_W and W_H is 1.6 mrad, 5.5 min in units of 2θ, or 1.0×10^{-2} mm^{-1} in units of $s = (2 \sin \theta)/\lambda_w$. The fwhm values are sufficiently narrow compared with the observed SAXS intensity distributions.

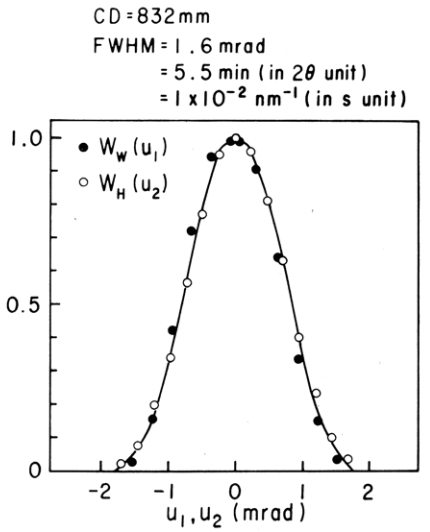

Figure 2. Measured slit weighting function $W(u_1,u_2) = W_W(u_1)W_H(u_2)$ for the optical arrangement shown in Figure 1.

In Figure 8, the intensity distribution with s is shown to be sharpest at $\psi = 0°$, having a minimum fwhm of 2.5×10^{-2} nm^{-1}, a value of that is still larger than the fwhm value of the weighting function. The intensity distribution with ψ at given s values can also be estimated from Figure 8. The fwhm for the azimuthal SAXS intensity distributions are much larger than that of the weighting function, e.g., the fwhm for the azimuthal angle dependence at $s \simeq 0.05$ nm^{-1} (near peak position) being estimated to be about 20° from Figure 8b for the particular crystallization conditions.

On the basis of the true scattered intensity distribution $I(s,\psi)$ one can determine the orientation distribution of lamellar normals. We assume that the system to be treated satisfies the following conditions: (i) orientation of the lamellar normal **n** is uniaxially symmetric with respect to the draw direction, and (ii) the lateral breadth B of the lamellae is much larger than the thickness D of the lamellae. Assumption ii requires that the scattering from a given stack of lamellae with a given orientation ψ_1 not significantly overlap in the azimuthal angle direction with that from a stack with different orientation ψ_2.

From the assumption ii, a stack of lamellae oriented at an angle ψ_1 with respect to the draw direction gives strong scattering when **s** is parallel to **n** (see Figure 3b). The scattered intensity from the stack $I_s(\mathbf{s}) = I_s(s,\psi)$ may be given by

$$I_s(s,\psi) \sim N(\psi_1)\delta(\psi-\psi_1)I_1(s) \qquad \text{(III-5)}$$

where $N(\psi_1)$ is the number of lamellae with their normals oriented at the angle ψ_1, and $I_1(s)$ is the scattering from the one-dimensional assembly of lamellae with the scattering vector **s** parallel to **n** (meridional scattering). The "meridional scattered intensity" $I_1(s)$ from the assembly depends on the thickness of lamellae D, the interlamellar spacing L and their distributions from mean values, the size of the stack parallel to **n**, and the electron-density difference between lamellae and their surrounding medium $(\rho_c - \rho_a)$.[41]

Although $I_1(s)$ and therefore $I_s(s,\psi)$ depend on detailed properties of the assembly such as regularity of interlamellar spacing, the integrated intensity with s at a given azimuthal angle ψ_1 becomes independent of the structure of the assembly.

$$Q(\psi) = \int_0^\infty s^2\, ds\, I_s(s,\psi) \sim N(\psi) \qquad \text{(III-6)}$$

It depends rather on the number of lamellae with their normals oriented at an angle ψ and $\rho_c - \rho_a$. The total number of lamellae is proportional to the total integrated intensity with s and ψ.

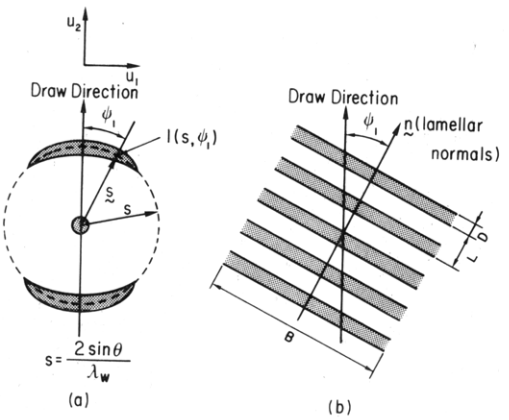

Figure 3. (a) Typical SAXS pattern in the plane perpendicular to the incident beam, and (b) a lamellar stack with normals **n** oriented at ψ_l with respect to the draw direction.

$$Q \equiv \int_0^\pi \sin\psi\, d\psi\, Q(\psi) = \int_0^\infty s^2\, ds \int_0^\infty \sin\psi\, d\psi\, I_s(s,\psi) \qquad \text{(III-7)}$$

$$\sim \int_0^\pi \sin\psi\, d\psi\, N(\psi) \qquad \text{(III-8)}$$

Consequently, the normalized orientation distribution function of the lamellar normals, $2\pi q_l(\psi)$, can be obtained by

$$2\pi q_l(\psi) = \frac{\int_0^\infty s^2\, ds\, I_s(s,\psi)}{\int_0^\infty s^2\, ds \int_0^\infty \sin\psi\, d\psi\, I_s(s,\psi)} \qquad \text{(III-9)}$$

It should be noted that the electron-density difference, which depends on crystallization conditions, is canceled out when the ratio of $Q(\psi)$ and Q is taken to obtain $2\pi q_l(\psi)$.

A rigorous measurement of $2\pi q_l$ requires the sample surface to be tilted with respect to the incident beam by the angle θ, one-half of the Bragg angle 2θ. Thus, for the SAXS intensity at the nth-order peak, one must tilt the sample by the angle θ_B given by

$$2\bar{L} \sin\theta_B = n\lambda_W \quad \text{or} \quad s_B\bar{L} = n \qquad \text{(III-10)}$$

where $\bar{L}$ is the average interlamellar spacing. Under this condition, the scattering vector **s** becomes parallel to **n** and therefore the scattering intensity is proportional to $N(\psi_1)$ (Figure 3). As seen in Figure 4 when the incident beam $\mathbf{s}_0$ is irradiated normal to the sample surface $(0u_1u_2)$, the SAXS intensity distribution with ψ on the Debye–Scherrer ring at $2\theta_B$ (satisfying eq III-10) depends on the distribution of the reciprocal vector $\mathbf{r}_l^*$ parallel to **n** on the reflecting circle R. In this case the reciprocal lattice vector or the vector **n** is inclined to the plane $0u_1u_2$ by the angle θ_B. Thus, $I(2\theta_B,\psi)$ does not rigorously represent $N(\psi)$, the distribution function of **n** on the circle C in the plane of $0u_1u_2$. In reality in the SAXS measurements θ_B is of the order of a few degrees at most, and therefore the tilting by the angle θ_B is not vitally important. The necessity for tilting is well-known in orientation measurements by wide-angle X-ray diffraction.[39]

IV. Experimental Results

1. Results Obtained by Photographic Method with Microdensitometry. Figure 5 represents typical WAXS patterns for rubber drawn by $\lambda = 1.6$ (top row) and $\lambda =$

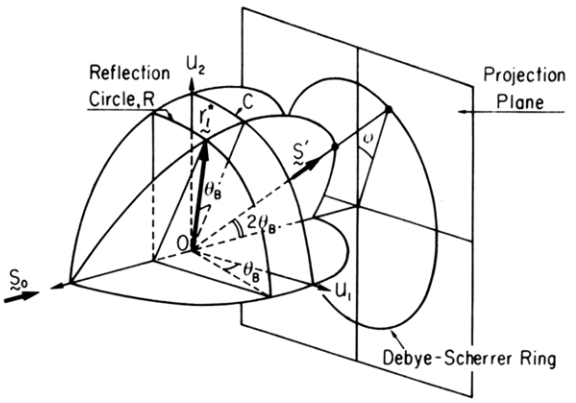

Figure 4. Debye–Scherrer ring in the projection plane (normal to $\mathbf{s}_0$, propagation direction of incident X-ray beam) and the reciprocal lattice vectors of the one-dimensional assembly $\mathbf{r}_i^*$ (parallel to the unit vector along lamellar normal **n**) which contribute to the Debye–Scherrer ring. The vectors $\mathbf{r}_i^*$ are on the reflecting circle R and are inclined by the angle θ_B (half the Bragg angle of the ring) with respect to the Ou_1u_2 plane (the sample surface, Ou_2, is parallel to the draw direction).

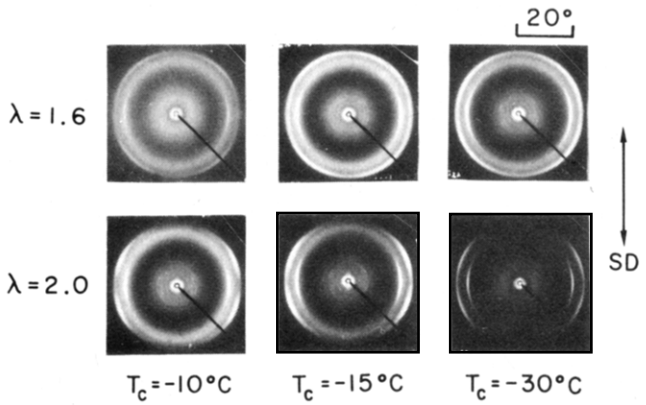

Figure 5. WAXS patterns for various crystallization temperatures T_c and draw ratios λ. Draw direction is vertical.

2 (bottom row) and crystallized at various T_c. Two strong diffractions were observed in each pattern: one from the (020) plane appearing at smaller 2θ on the equator, and another from the (110) plane at larger 2θ and off-equatorial position. The tilt angle α between the equator and the azimuthal angle at which the (110) diffraction reaches a maximum decreases with increasing λ at a given T_c but does not depend upon T_c at a given λ (Figure 7b). The width of each diffraction with respect to the azimuthal angle decreases with increasing λ at a given T_c and with increasing T_c at a given λ, although the tilt angle α hardly changes with T_c. These results indicate that the degree of *c*-axis (chain axis) orientation increases with increasing draw ratio (i.e., with increasing orientation of amorphous chains) at a given T_c and increases with increasing T_c at a given λ.

Figure 6 shows typical SAXS patterns obtained at various values of λ and T_c with horizontal draw direction (SD). SAXS generally produces typical two-point patterns oriented in the meridional direction (i.e., along the draw direction (SD)). Thus, crystallization produces oriented arrays of crystallites with well-defined long periods probably arising from a stack of lamellar platelets with their normals oriented along SD.

The width of the two-point patterns perpendicular to SD ("lateral width") decreases with increasing λ at a given T_c and with increasing T_c at a given λ. These results are primarily attributed to an increasing degree of orientation of the lamellar normals, in agreement with WAXS data.

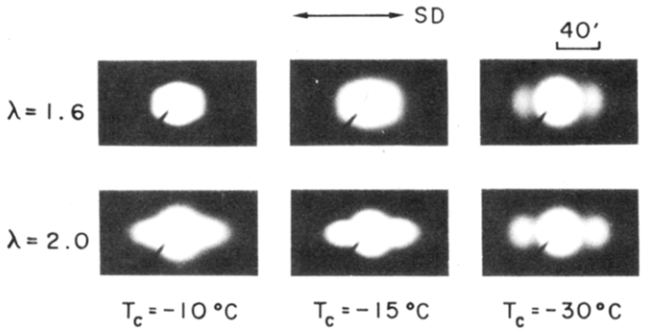

Figure 6. SAXS patterns for various T_c and λ. Draw direction is horizontal.

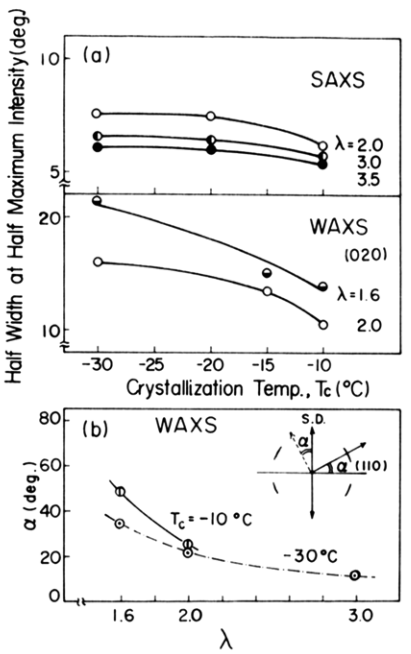

Figure 7. (a) Half-width of azimuthal angle dependence of the SAXS and WAXS intensity of (020) reflection vs. crystallization temperature. (b) Tilt angle α between the (110) reciprocal lattice vector and horizontal plane at T_c = 260 and 240 K vs. draw ratio.

The SAXS and WAXS patterns were time-averaged over a period of X-ray exposure. The patterns in Figures 5 and 6 were taken after a sufficient time of isothermal crystallization (typically 3 h) that the change of the long spacing of the SAXS patterns with time leveled off and the crystallinity estimated from WAXS reached a maximum value. The SAXS and WAXS studies on the kinetics of oriented crystallization will be reported in detail in a forthcoming paper.[25]

Figure 7 shows results of microdensitometric scanning of the WAXS and SAXS patterns of Figures 5 and 6. The results quantitatively confirmed the conclusions obtained from Figures 5 and 6.

2. Results Obtained with a Position-Sensitive Proportional Counter (PSPC). a. SAXS. Figure 8a represents typical SAXS profiles measured at various azimuthal angles ψ for the following crystallization conditions: λ = 2, T_c = 263 K. The profiles were measured with a stationary PSPC by rotation of the sample direction SD; ψ = 0 corresponds to scattering along SD (designated hereafter as "meridional scattering") with 100-s exposure to X-rays for samples crystallized for sufficient times that the long identity periods and crystallinity (measured by SAXS and WAXS) reached constant values.[25] In Figure 8a the origin of each profile was shifted vertically to avoid overlapping.

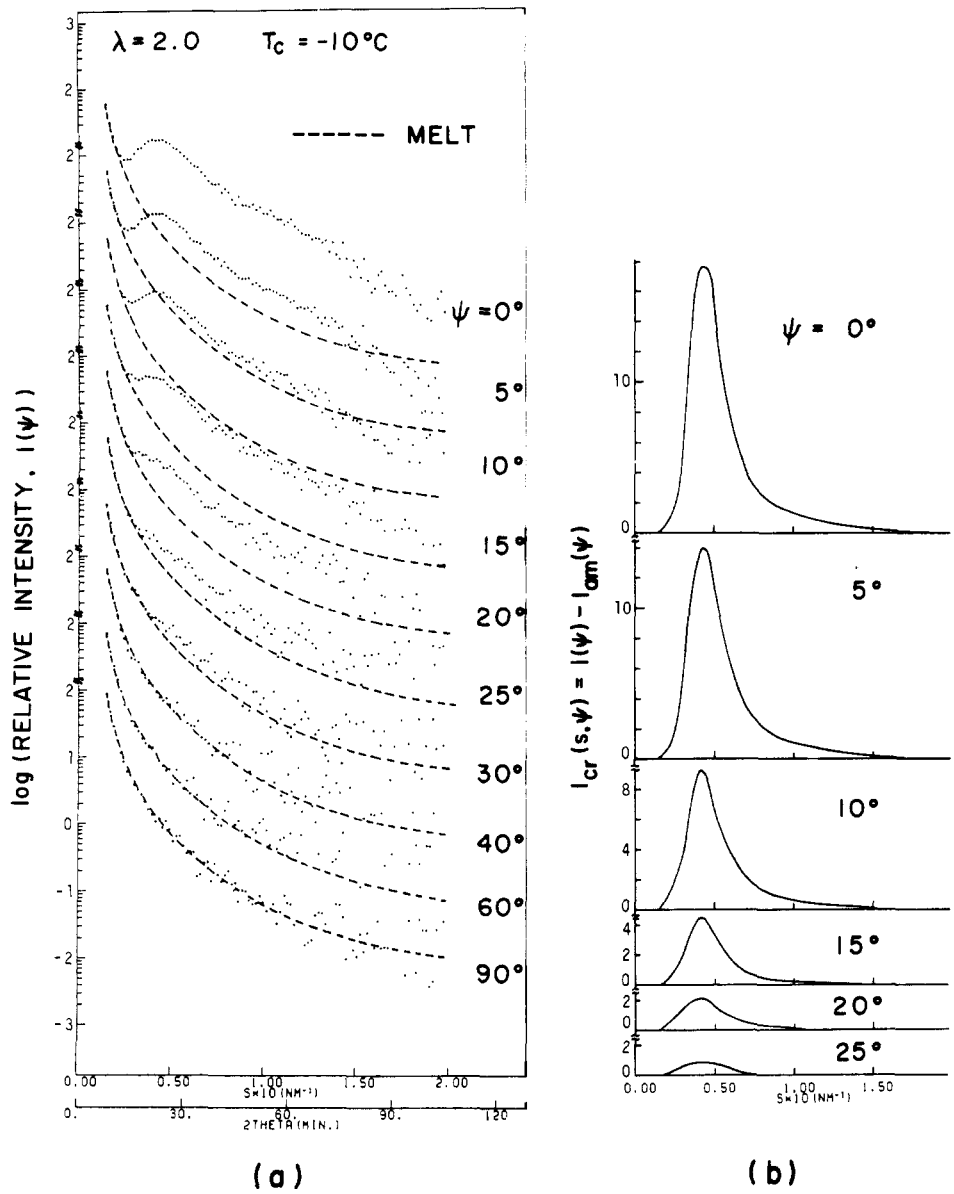

Figure 8. (a) Typical SAXS profiles at various azimuthal angles ψ for a specimen crystallized at $\lambda = 2.0$ and $T_c = 260$ K (dots) and SAXS profiles for the same specimen at $\lambda = 2.0$ at room temperature, i.e., above melting point (broken lines). (b) Profiles for the excess scattering $I_{cr}(s,\psi)$ due to crystallization at various ψ. $s = 2 \sin \theta/\lambda_w$, 2θ and λ_w being the scattering angle and wavelength of the X-rays.

The scattering intensity distributions $I_{am}(s,\psi;\lambda,T=25\ ^\circ C)$ from the molten rubbers at a given λ were also measured as functions of ψ at room temperature (which is higher than the melting point of all the stretched specimens). At a given ψ the profile drawn by dots and that drawn by the broken curve correspond to SAXS curves respectively after and before crystallization. These SAXS curves were obtained after introduction of a series of corrections. First the data were corrected for the absorption; then air and parasitic scattering were subtracted from the corrected data. The data thus obtained were finally corrected for diffuse scattering arising from thermal density fluctuations.

In order to obtain scattering from the crystallized part of the polymer $I_{cr}(s,\psi;T_c,\lambda)$, from the corrected scattered intensity after crystallization $I(s,\psi;T_c,\lambda)$, the scattered intensity $I_{am}(s,\psi;\lambda,T=25\ ^\circ C)$ arising from inhomogeneities of the amorphous phase was subtracted. Sulfur and some additives to cure the rubber as well as inhomogeneity in cross-link density may be sources of the inhomogeneities.

$$I_{cr}(s,\psi;T_c,\lambda) = I(s,\psi;T_c,\lambda) - I_{am}(s,\psi;\lambda) \qquad \text{(IV-1)}$$

The intensity I_{cr}, which reflects "excess scattering" due to the crystallization, was also plotted in Figure 8b for various ψ.

From Figures 8a,b it is obvious that the peak positions are essentially independent of ψ and the peak intensity decreases with increasing ψ, the effects of which may be primarily associated with orientation distribution of the lamellar normals. Normalized orientation distribution of the lamellar normals, $q_l(\psi)$, was estimated from the excess scattering I_{cr} by using the following relationship, according to the principle described in section III:

$$2\pi q_l = \frac{\int_0^\infty s^2\, ds\, I_{cr}(s,\psi;T_c,\lambda)}{\int_0^\infty s^2\, ds \int_0^\infty \sin\psi\, d\psi\, I_{cr}(s,\psi;T_c,\lambda)} \qquad \text{(IV-2)}$$

Equation IV-2 is valid for orientation distribution of the lamellar normals, which is uniaxial with respect to SD. The assumption of a uniaxial orientation distribution should be a good approximation.

Figure 9 shows normalized orientation distributions thus determined for nine sets of crystallization conditions (λ,T_c).

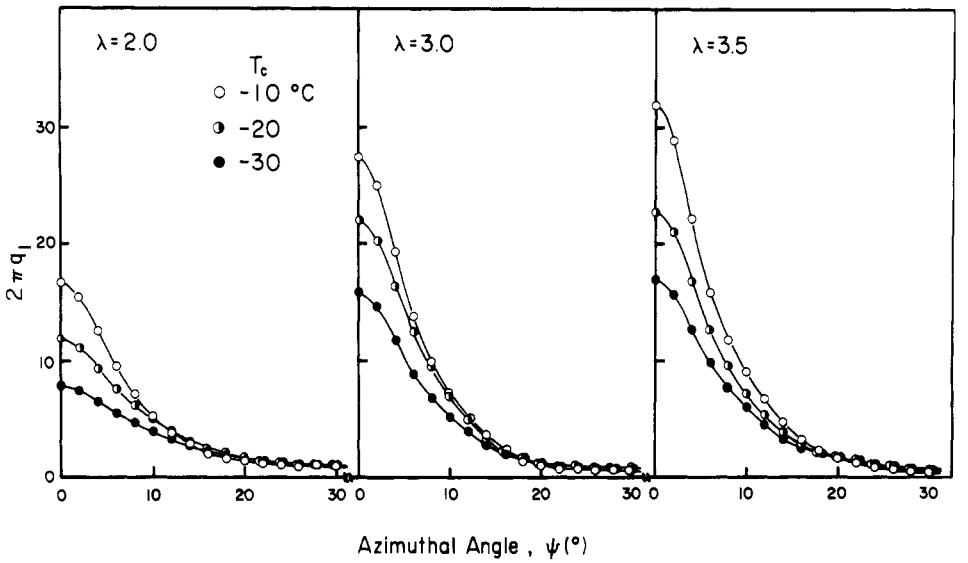

Figure 9. Normalized orientation distribution functions $2\pi q_l$ for the lamellar normal for various crystallization conditions λ, T_c (indicated).

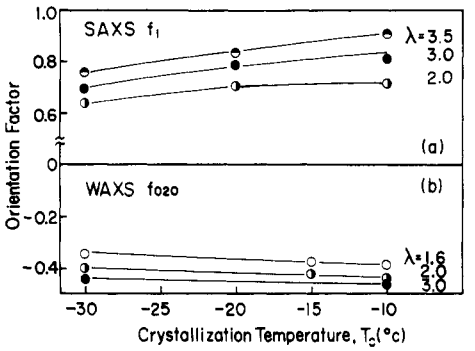

Figure 10. Orientation factors $f_l = (3\langle\cos^2\psi_l\rangle - 1)/2$ for the lamellar normal (a), and $f_{020} = (3\langle\cos^2\psi_{020}\rangle - 1)/2$ for the reciprocal lattice vector of the (020) plane (b) as a function of T_c at various λ.

The orientation distribution function $2\pi q_l$ becomes increasingly sharp with increasing T_c at a given λ, which can be interpreted by the molecular theory of oriented crystallization (see section V). The orientation factor, f_l, of the $2\pi q_l$ distribution was also calculated with the relation

$$f_l = [3\langle\cos^2\psi_l\rangle - 1]/2 \qquad \text{(IV-3a)}$$

$$\langle\cos^2\psi_l\rangle = \int_0^\pi \sin\psi\, d\psi\, 2\pi q_l(\psi)\cos^2\psi \qquad \text{(IV-3b)}$$

The results are plotted in Figure 10a. The orientation factor f_l increases with increasing both T_c and λ.

b. WAXS. Figure 11 shows the WAXS profiles at various ψ measured with PSPC by rotation of samples crystallized at λ = 3.0 and T_c = 243 K after a period of 1 h required for the sample to attain equilibrium crystallinity.[25] The measured profile at each ψ (shown by dots) was decomposed into a broad amorphous halo with its maximum intensity at 2θ = 19.7°, a series of sharp diffraction peaks from crystal planes (020) (2θ = 18.7°), (110) (2θ = 22.3°), and (030) (2θ = 27.8°), and the background scattering (shown by straight line). Decomposition of the profile was done as a linear combination of Gaussian, Lorentzian, and linear functions. Coefficients of this combination, peak heights and peak widths, were found to produce the best fit by a least-squares method.

From the decomposed profile from (*hkl*) crystal planes, $I_{hkl}(s,\psi;T_c,\lambda)$, one can estimate the normalized orientation distribution function $q_{hkl}(\psi)$ of the reciprocal lattice vectors $\mathbf{r}^*_{hkl}$ in the same manner as the function $2\pi q_l$ in eq IV-2.

$$2\pi q_{hkl} = \frac{\int_0^\infty s^2\, ds\, I_{hkl}(s,\psi;T_c,\lambda)}{\int_0^\infty s^2\, ds \int_0^\infty \sin\psi\, d\psi\, I_{hkl}(s,\psi;T_c,\lambda)} \qquad \text{(IV-4)}$$

The normalized orientation distribution functions $2\pi q_{hkl}$ thus estimated are plotted in Figure 12 for the reciprocal lattice vectors of the (110) and (020) planes for specimens isothermally crystallized at various (λ,T_c). It is clearly shown that orientation distribution functions become sharper with increasing T_c at a given λ, and with increasing λ at a given T_c, in parallel to the results obtained from SAXS. The orientation factor, f_{020}, of the orientation distribution function $2\pi q_{020}$ was also estimated, and presented in Figure 10b, as

$$f_{hkl} = [3\langle\cos^2\psi_{hkl}\rangle - 1]/2 \qquad \text{(IV-5a)}$$

$$\langle\cos^2\psi_{hkl}\rangle = \int_0^\pi d\psi\, \sin\psi\, 2\pi q_{hkl}(\psi;T_c,\lambda)\cos^2\psi \qquad \text{(IV-5b)}$$

The values of f_{020} are negative and decrease to $-1/2$ with increasing T_c and λ, which again corresponds to increasing orientation of the *c* axis.

c. Relation between the Second Moments of Orientation Distributions As Measured by SAXS and WAXS. In this section we estimate the second moment of the orientation distribution function of the *c* axis ($\langle\cos^2\psi_c\rangle$) from the orientation distributions of (110) and (020) reciprocal lattice vectors and compare the results with the second moment of the lamellar normals as estimated by SAXS (see section IV-2-a). The angle ψ_c is the angle between SD and the *c* axis.

The principle of estimating the orientation factor of crystal axes was first developed by Stein[29] for an orthorhombic system. Wilchinsky[30] generalized the method for more complicated crystal structures and gave formulas relating the moment of the reciprocal lattice vector $\mathbf{r}^*_{hkl}$ ($\langle\cos^2\psi_{hkl}\rangle$) to the moments of the crystal axes ($\langle\cos^2\psi_m\rangle$, *m* representing the *a*, *b*, or *c* axis):

$$\langle\cos^2\psi_{hkl}\rangle = e^2\langle\cos^2\psi_U\rangle + f^2\langle\cos^2\psi_b\rangle + g^2\langle\cos^2\psi_c\rangle + 2ef\langle\cos\psi_U\cos\psi_b\rangle + 2ge\langle\cos\psi_c\cos\psi_U\rangle + 2fg\langle\cos\psi_b\cos\psi_c\rangle \qquad \text{(IV-6)}$$

cis-1,4-Polybutadiene forms of monoclinic crystal with *a*

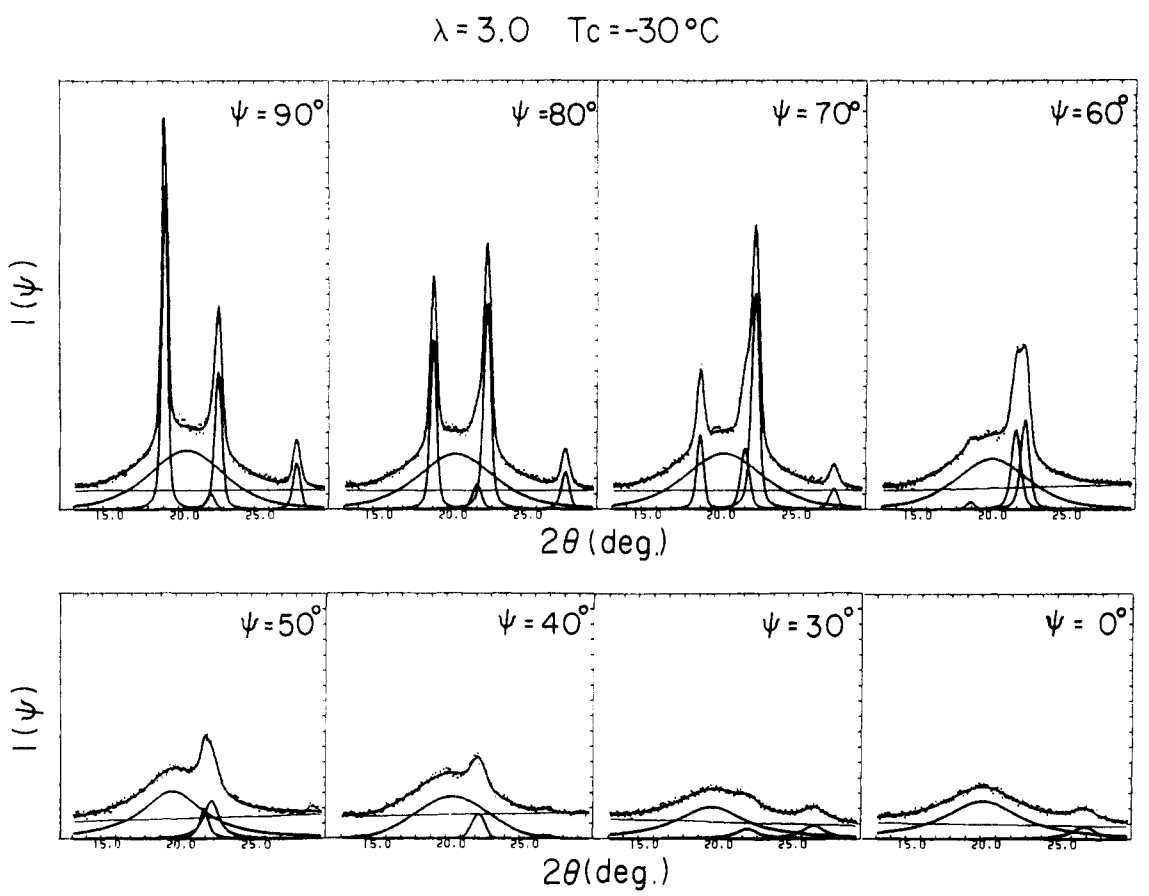

Figure 11. Typical WAXS profiles at various azimuthal angles ψ for the specimen crystallized at $\lambda = 3.0$ and $T_c = 240$ K.

= 0.464 nm, b = 0.950 nm, c = 0.860 nm, $\alpha = \gamma = 90°$, and $\beta = 109°$. In eq IV-6 the axis U was chosen such that the three axes b, c, and U become orthogonal (see Figure 13). The quantities e, f, and g are the direction cosines of $\mathbf{r}^*_{hkl}$ with respect to U, b, and c.

Applying eq IV-6 to (020) and (110) reciprocal lattice vectors, in the monoclinic system

$$\langle \cos^2 \psi_{020} \rangle = \langle \cos^2 \psi_b \rangle \quad \text{(IV-7)}$$

$$\langle \cos^2 \psi_{110} \rangle = e^2 \langle \cos \psi_U \rangle + f^2 \langle \cos^2 \psi_b \rangle \quad \text{(IV-8)}$$

and noting the mutual orthogonality of b, c, and U

$$\langle \cos^2 \psi_c \rangle + \langle \cos^2 \psi_b \rangle + \langle \cos^2 \psi_U \rangle = 1 \quad \text{(IV-9)}$$

one can estimate $\langle \cos^2 \psi_c \rangle$ from the measured quantities $\langle \cos^2 \psi_{020} \rangle$ and $\langle \cos^2 \psi_{110} \rangle$, and the quantities e and g can be estimated from the crystal structure.

Figure 14 represents a comparison between $\langle \cos^2 \psi_l \rangle$ (solid lines) and $\langle \cos^2 \psi_c \rangle$ (broken lines) at various T_c and λ. We note that $\langle \cos^2 \psi_l \rangle$ is larger than $\langle \cos^2 \psi_c \rangle$, which might be due to a "chain-tilting" effect as depicted in Figure 15. If the chain axis c is normal to the basal plane as in Figure 15a, then the two moments should be identical. If c is inclined to the basal plane (Figure 15b), $\langle \cos^2 \psi_l \rangle$ can be greater than $\langle \cos^2 \psi_c \rangle$. However, model b seems to be less probable than model c, in which the chain axis, rather than the lamellar normal, is parallel to SD, in view of the mechanism by which external mechanical energy is transferred through polymer material. In model c, $\langle \cos^2 \psi_l \rangle$ is smaller than $\langle \cos^2 \psi_c \rangle$, in contradiction to the observation. An alternative explanation is an error in estimating $\langle \cos^2 \psi_l \rangle$, especially one associated with assessment of the scattering intensity I_{cr} based on eq IV-1. The validity of eq IV-1 may be questioned, and the discrepancy between the two moments should be further investigated.

V. Theoretical Analysis

Crystallite orientation observed in a polymer sample results from a complex interplay of thermodynamic and kinetic factors. We shall consider two asymptotic theoretical models: (i) one assuming an equilibrium system where orientation is controlled solely by thermodynamics and (ii) a system where each crystal maintains the original orientation of its nucleus and crystal orientation distribution depends on the kinetics of nucleation. Being aware of limitations involved in the asymptotic models we do not attempt quantitative comparison of the theory with experiment; it seems worthwhile, though, to check how the asymptotic models reproduce qualitative features of our experimental data.

1. Equilibrium Theory. We assume a regular network of "phantom" Gaussian chains. Crystallization transforms any crystallizing chain into a stiff crystalline part and a flexible amorphous part. Both are characterized by some end-to-end vectors and contour lengths. Free energy change due to this transformation includes free energy of phase transition, free energy of conformational changes in the amorphous part of the system, and free energy of crystallite interactions. Interactions neglected, the free energy change due to crystallization of one chain is[21]

$$\Delta F = \Delta F_{\text{free}} + \tfrac{3}{2}kT\left[\frac{S\mathbf{H}^2(\psi) - 2\mathbf{H}(\psi)\mathbf{R} + \Gamma\mathbf{R}^2}{1 - S\Gamma} + \ln(1 - S\Gamma)\right] \quad \text{(V-1)}$$

where S is the degree of crystallinity for a single chain, $\mathbf{R}$ is the reduced vector of the crystallite (divided by mean square end-to-end distance of the uncrystallized free chain), $\mathbf{H}(\psi)$ is the reduced end-to-end vector of the uncrystallized (mother) network chain, Γ is the parameter of network flexibility, and ΔF_{free} is the free energy of

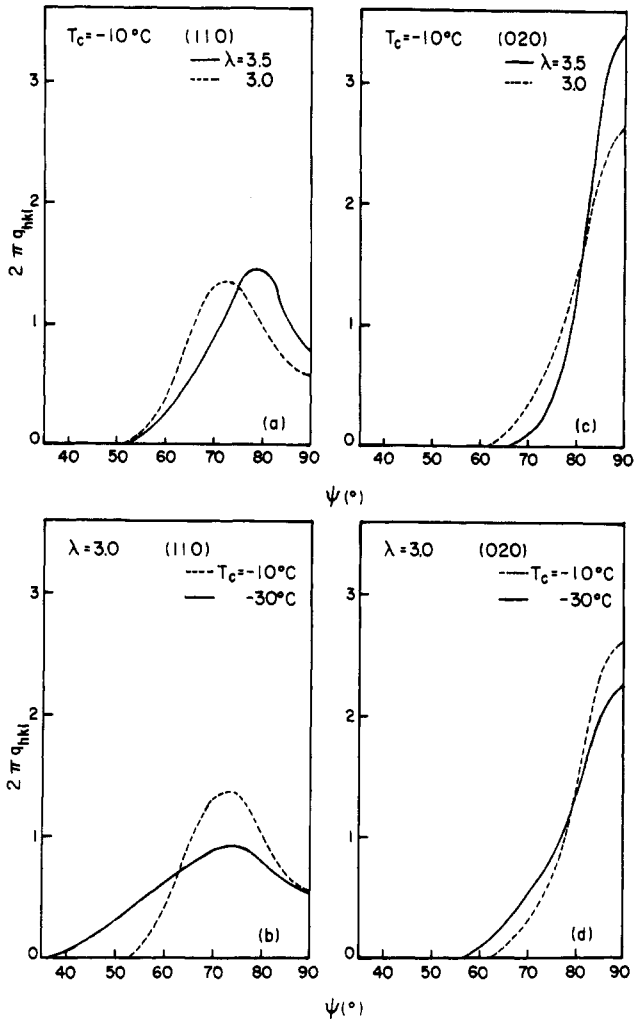

Figure 12. Normalized orientation distribution functions $2\pi q_{hkl}$ for the reciprocal lattice vectors of the (110) and (020) planes at various crystallization conditions λ, T_c (indicated).

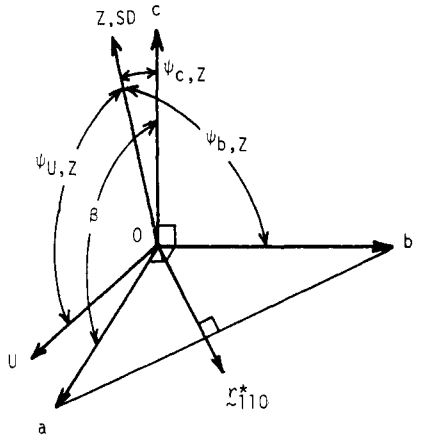

Figure 13. Relationship between crystallographic axes (*a*, *b*, and *c*), *U* axis, and *Z* axis. *Z* axis is parallel to stretching direction (SD) and *U* axis lies in the plane *a*O*c* and is perpendicular to *c* axis (O*bcU* forms an orthogonal system). $\beta = 109°$.

crystallization of an isolated chain, including bulk free energy change $-(3/2)kTSu$ and free energy of folding q.

We introduce simple assumptions concerning crystallite morphology. Each crystallite consists of a certain number of "single-chain crystallites". We assume that these "single-chain" elements are of either fully extended-chain type ($R = SN_s^{1/2}$) or folded-chain type with one symmetric fold of negligibly small width ($R \approx 0$). Large crystallites generally have a mixed morphology admitting special cases

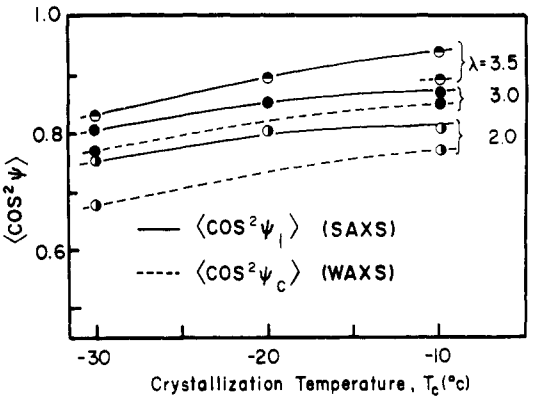

Figure 14. Comparison of the second moments of the orientation distribution functions of the lamellar normal, $\langle\cos^2\psi_l\rangle$, and of the *c* axis, $\langle\cos^2\psi_c\rangle$, estimated from $\langle\cos^2\psi_{110}\rangle$ and $\langle\cos^2\psi_{020}\rangle$ using eq IV-7–IV-9.

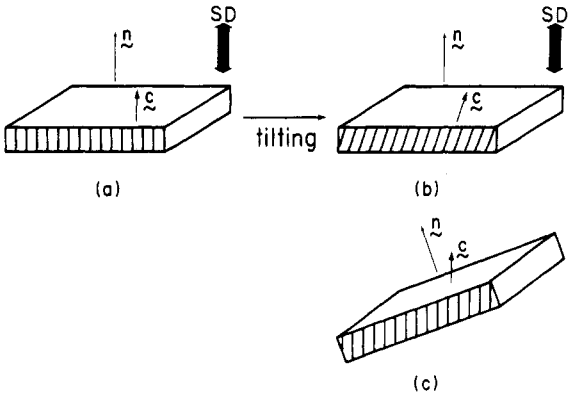

Figure 15. Relation between the unit vectors along lamellar normal **n** and *c* axis: (a) **n** and **c** parallel to stretching direction (SD); (b) **n** parallel to SD; (c) **c** parallel to SD.

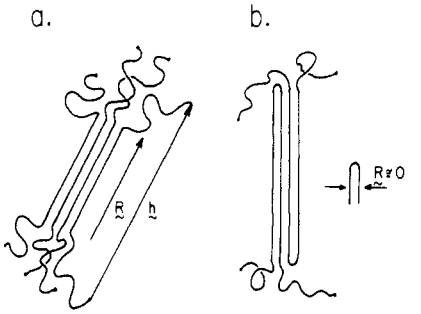

Figure 16. Model morphologies of crystallites: (a) bundlelike crystallites; chain vectors parallel to crystallite end-to-end vector, (b) folded-chain crystallites; each chain contributes a single fold of negligibly small width and random orientation.

of purely bundlelike or folded-lamellar morphology (see Figure 16). It is also assumed that the form of a single-chain crystallite is determined by molecular deformation of the mother chain; this means that strongly elongated chains contribute extended-chain crystallites while folded single-chain crystallites come from relaxed chains. A precise criterion for determination of the type and size of a single-chain crystallite is the minimum free energy of crystallization of a particular chain. One has to minimize the free energy from eq V-1 with respect to crystallinity variables (S, R), for both fully extended and folded morphologies, and then choose a morphology corresponding to the lower free energy value. For any chain this procedure yields most probable morphology and size of the crystallized part. An obvious result is that extended-chain crystallites are preferentially oriented along the end-to-end vector of the chain, while folded crystallites are oriented

randomly (ΔF independent of $\mathbf{R}$). Minimization gives simple expressions for the equilibrium degree of crystallinity of a single chain

$$S^* = \frac{1}{\Gamma} + \frac{1}{2\mu} - \frac{(1 + 4\mu H^2(\psi)/\Gamma^2)^{1/2}}{2\mu} \qquad \text{(V-2)}$$

for folded-chain crystallites, and

$$S^* = \frac{1}{\Gamma} + \frac{1}{2(\mu + N_s)} - \frac{[1 + 4(\mu + N_s)(H(\psi) - N_s^{1/2})^2/\Gamma^2]^{1/2}}{2(\mu + N_s)} \qquad \text{(V-3)}$$

for extended-chain crystallites, with the constraint $0 \leq S^* \leq 1$.

Equations V-2 and V-3 provide relations between chain orientation and equilibrium size of single-chain crystallites; they will be used later for determining orientation distribution functions.

Let us define the orientation distribution function of crystallites as a function whose value at a given angle ψ is proportional to the amount of crystallized material oriented at ψ. It is assumed that orientation of a crystallite is described by the angle ψ between crystallite c axis and stretching direction. Crystallized material is made of all single-chain contributions and consists of folded and extended single-chain elements. Apart from different sizes and free energies, the two types of crystallites also differ in their orientation distributions since extended-chain crystallites are preferentially oriented along end-to-end vectors of their mother chains, and folded-chain crystallites are randomly oriented. Consequently, the orientation distribution function of crystallites must have the

$$W_c(\psi) = (\text{constant}) \times \left[S^*_B(\psi)N(\psi) + \tfrac{1}{2}\int_0^\pi \sin\psi'\, d\psi'\, S^*_F(\psi')N(\psi')\right] \qquad \text{(V-4)}$$

where $N(\psi)$ is the number density of chains oriented at ψ, and S^*_B and S^*_F are chain degrees of crystallinity for bundlelike and folded morphologies ($S^*_B = 0$ when folded-chain morphology is preferred, $S^*_F = 0$ otherwise). The number density of chains for affine uniaxial deformation (cf. ref 8) is

$$N(\psi) = \tfrac{1}{2}[\lambda^2 - (\lambda - 1/\lambda^2)\cos^2\psi]^{-3/2} \qquad \text{(V-5)}$$

provided that the orientation distribution of chains in the undeformed state is isotropic ($N_0(\psi) = {}^1/_2$).

Equation V-5 provides the required expression for the orientation distribution function of the crystallite c axes in the crystallized sample at equilibrium. The problem of orientation distribution functions for other crystallographic axes will be discussed separately.

2. Kinetic Theory. The following considerations are based on the theory of crystal nucleation from oriented asymmetric elements.[31-33] Cylindrical elements are assumed (each one characterized by its radius, r, length, l, and orientation angle to stretching direction ψ). The theory stipulates consistent orientation of a growing cluster and colliding single element as a necessary condition for cluster growth. The effective driving force of cluster growth, $\Delta\tilde{F}$, becomes dependent on cluster (nucleus) orientation, ψ

$$\Delta\tilde{F}(r,l,\psi) = \Delta\tilde{F}_0(r,l) - kT\left(\frac{\pi r^2 l}{v_0} - 1\right)\ln\chi(\psi) \qquad \text{(V-6)}$$

where $\Delta\tilde{F}_0$ is free energy of cluster formation in an isotropic system; $v_0 = \pi r_0^2 l_0$ is the volume of a single element, and $\chi(\psi)$ is proportional to the probability of finding a single element oriented at χ within some finite tolerance range Δ

$$\chi(\psi) = (4\pi/\Delta)\int_\Delta w_{am}(\psi')\sin\psi'\, d\psi' \cong 4\pi w_{am}(\psi) \qquad \text{(V-7)}$$

($w_{am}(\psi)$ denotes the orientation distribution function of single elements).

The consequence of eq V-6 is a nonuniform orientation distribution of steady-state nucleation rate, $\dot{N}_{st}$, and cluster angular density, w_{cl}

$$d\dot{N}_{st}/d\psi = (\text{constant})\chi(\psi)w_{am}(\psi)\exp[-\Delta\tilde{F}(r^*,l^*,\psi)/kT] \qquad \text{(V-8)}$$

$$w_{cl}(r,l,\psi) = (\text{constant})w_{am}(\psi)\exp\left[-\frac{\Delta\tilde{F}(r^*,l^*,\psi)}{kT}\right] \times \left\{1 - \frac{\int_{r_0}^{r} r^2\, dr \int_{l_0}^{l} dl\, \exp[\Delta\tilde{F}(r,l,\psi)/kT]}{\int_{r_0}^{\infty} r^2\, dr \int_{l_0}^{\infty} dl\, \exp[\Delta\tilde{F}(r,l,\psi)/kT]}\right\} \qquad \text{(V-9)}$$

The free energy $\Delta\tilde{F}(r^*,l^*,\psi)$ appearing in eq V-8 refers to a cluster with critical dimensions corresponding to the saddle point of the function $\Delta F(r,l)$

$$\left.\frac{\partial\Delta F(r,l,\psi)}{\partial r}\right|_{\substack{r=r^*\\l=l^*}} = \left.\frac{\partial\Delta F(r,l,\psi)}{\partial l}\right|_{\substack{r=r^*\\l=l^*}} = 0 \qquad \text{(V-10)}$$

We define a "kinetically determined crystal orientation distribution function" as a normalized distribution of clusters with critical size r^*, l^*

$$W_c(\psi) = w_{cl}(r^*,l^*,\psi) \qquad \text{(V-11)}$$

Identification of the crystal orientation distribution with that of critical clusters means that critical nuclei once formed retain their orientation in subsequent growth.

For the cluster critical size the integral term in eq V-9 can be approximated by a constant of the order of ${}^1/_2$. Then

$$W_c(\psi) = (\text{constant})w_{am}(\psi)\exp\left[-\frac{\Delta\tilde{F}(r^*,l^*,\psi)}{kT}\right] \qquad \text{(V-12)}$$

Now, the expression for free energy of formation of a cylindrical cluster is assumed in the form

$$\Delta\tilde{F}(r,l,\psi) = 2\pi r^2\sigma_e + 2\pi rl\sigma_s + \pi r^2 l[\Delta f - (kT/v_0)\ln\chi(\psi)] \qquad \text{(V-13)}$$

where σ_e and σ_s are end and side surface free energy densities, and Δf is bulk density of crystallization free energy. Then, the orientation distribution function of crystallites resulting from eq V-10 and V-12 is

$$W_c(\psi) = C\exp[-8\pi\sigma_e\sigma_s^2/(D^2(\psi)kT)] \qquad \text{(V-14)}$$

where C is a normalization constant, and the orientation-dependent function $D(\psi)$ is given by

$$D(\psi) = \Delta f - \frac{kT}{v_0}\ln\chi(\psi) = \Delta f - \frac{kT}{v_0}\ln[4\pi w_{am}(\psi)] \qquad \text{(V-15)}$$

Assumption of Kuhn–Grün statistics for segment orientation leads, under uniaxial deformation, to

$$\Delta f = \Delta f|_{\lambda=1} - \frac{kT}{v_0}\frac{1}{2N_s}\left(\lambda^2 + \frac{2}{\lambda} - 3\right) \qquad \text{(V-16)}$$

$$w_{am}(\psi) = \frac{1}{4\pi}\left[1 + \frac{1}{N_s}\left(\lambda^2 - \frac{1}{\lambda}\right)\frac{3\cos^2\psi - 1}{2} + O(N_s^{-2})\right] \qquad \text{(V-17)}$$

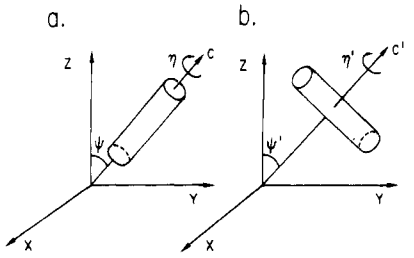

Figure 17. Angles describing crystallite orientation: (a) related to c-axis orientation (ψ,η); (b) related to an axis perpendicular to c axis (ψ',η').

Equations V-16 and V-17 provide approximate expressions for Δf and w_{am}. Equation V-16 is derived under the condition that the free energy of macroscopic deformation is uniformly distributed among all chains, and eq V-17 is the first-order approximation of the orientation distribution function postulated in ref 37. The bulk free energy density of crystallization of an undeformed sample, $\Delta f|_{\lambda=1}$, is related to the ideal melting point, T_m^0, and the crystallization temperature T_c.

$W_c(\psi)$ from eq V-14 provides the required orientation distribution of the crystallite c axes.

3. Orientation Distribution of Axes Perpendicular to the c Axis. A complete description of crystallite orientation requires the three Euler angles ψ, η, ϕ. Uniaxial symmetry reduces the problem to two angles, say ψ and η, which describe the orientation of the c axis and the rotation around the c axis, respectively. Let us denote two-angle distribution function by $W(\psi,\eta)$. Then, the orientation distribution function for the c axis is given by

$$W_c(\psi) = \int_0^{2\pi} W(\psi,\eta)\, d\eta \qquad \text{(V-18)}$$

Similarily, the orientation distribution of an axis perpendicular to the c axis is

$$W_\perp(\psi') = \int_0^{2\pi} W(\psi(\psi',\eta'),\eta(\psi',\eta'))\, d\eta' \qquad \text{(V-19)}$$

where ψ' and η' characterize the orientation of the considered axis and rotation around this axis, respectively (see Figure 17). When $W(\psi,\eta)$ is independent of η (free rotation around the c axis) $W(\psi',\eta')$ is identical for all axes perpendicular to the c axis. A possible source of η-dependent distribution is provided by the strain energy of anisotropic crystallites in a stress field, which exists in a deformed network.[34,35] Anisotropically elastic crystals tend to orient in a stress field to minimize their strain energy. This strain energy contributes to the free energy of crystallization $\Delta\tilde{F}$ and to the driving force for nucleation, $\Delta\tilde{F}$. Therefore, anisotropic elasticity may affect crystal orientation in both the equilibrium and the kinetic theories. As a result of such perturbation one can expect a modified c axis distribution and a η-dependent distribution $W(\psi,\eta)$. Using this concept we assume the orientation distribution $W(\psi,\eta)$ in a model form

$$W(\psi,\eta) = W_c(\psi)w(\eta;\psi) \qquad \text{(V-20)}$$

where the normalized distribution of the rotational angle η at constant ψ is given by

$$w(\eta;\psi) = C \exp[-A(\cos^2\xi - 2|\cos\xi \cos\xi^*|)] \qquad \text{(V-21)}$$

$$\cos\xi = \sin\delta \sin\psi \cos(\eta + \kappa_0)$$

$$\cos^2\xi^* = 1/(\lambda^2 + \lambda + 1)$$

In the above formulas ξ is an angle between the axis whose orientation with respect to crystallographic axes (either c and the reciprocal lattice vector of (110) or c and the reciprocal lattice vector of (020)) is characterized by angles δ, κ_0 (see Figure 18, k axis), and the stretching direction. The property of $w(\xi) = w(\eta;\psi)$ is that the most probable value of ξ is ξ^* which corresponds to the direction along which there is no effective deformation. Thus, a preferred orientation of the crystallite is that with the k-axis pointing along ξ^*. Parameter A is related to the intensity of the stress field.

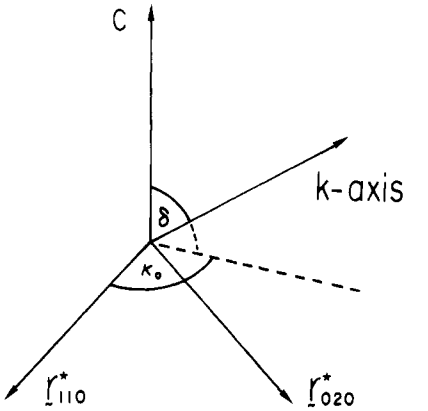

Figure 18. Angles δ, κ_0 defining position of k axis with respect to c axis and reciprocal lattice vectors (110) and (020).

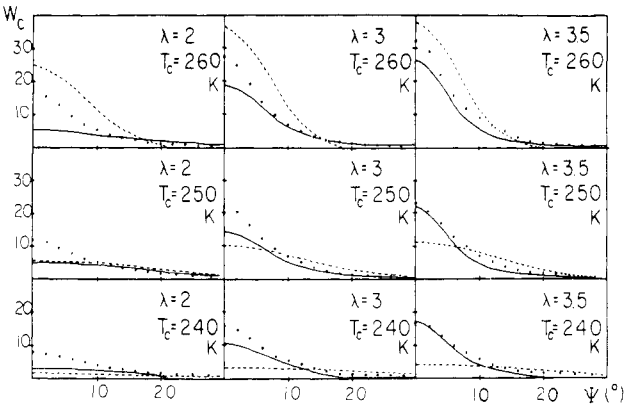

Figure 19. Orientation distribution functions of crystallite c axis at different crystallization conditions T_c, λ (indicated). Theoretical results—equilibrium theory (continuous lines) and kinetic theory (dashed lines); experimental (SAXS)—dots.

The model orientation distribution assumed above will be used in numerical calculations for simulation of the distribution of crystal axes perpendicular to the c axis.

VI. Theoretical vs. Experimental Orientation Distributions

Calculated orientation distribution functions for the c axis and the (110) and (020) reciprocal lattice vectors are compared with experimental data. The comparison is qualitative rather than quantitative because our theory is based on asymptotic models, and some of the required parameters can be only roughly estimated.

The following values of parameters were used: number of statistical segments in a network chain $N_s = 100$ (average molecular weight between cross-links 9×10^3), ideal melting temperature $T_m^0 = 270$ K, enthalpy of melting per mole of statistical segments 9.247×10^3 J/mol, enthalpy density 1.71×10^2 J/cm^3,[8] volume of a single kinetic element $v_0 = 2.9 \times 10^{-22}$ cm^3, surface free energy parameter $\sigma_s^2\sigma_e = 2 \times 10^{-18}$ J^3/cm^6, free energy of fold formation $q = 4.5 \times 10^{-27}$ J,[38] parameter of network flexibility $\Gamma = {}^1/_2$.[21]

The orientation distribution functions of the crystallite c axis predicted by equilibrium and kinetic theories are presented in Figure 19. It is apparent that both theories

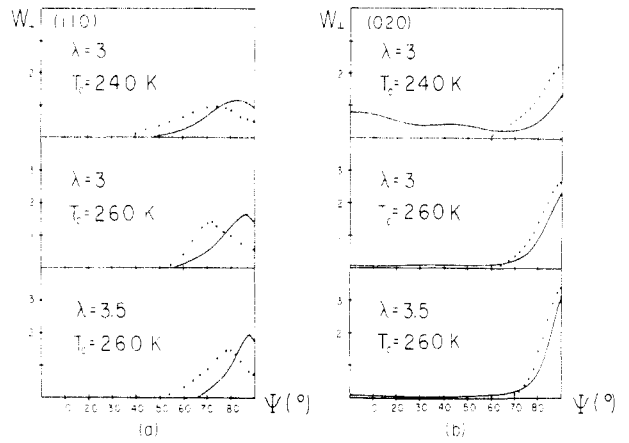

Figure 20. Orientation distribution functions of (a) (110) reciprocal lattice vector and (b) (020) reciprocal lattice vector. Theoretical predictions based on eq V-19–V-21 with parameter values $A = 20$, $\delta = 90°$, $\kappa_0 = 0°$ for (110) plane and $\kappa_0 = 66°$ for (020) plane—continuous lines. Experimental results (WAXS)—dots.

predict the observed sharpening of the distribution functions with increasing deformation ratio λ and/or with increasing crystallization temperature, T_c. In the kinetic theory this is related to the function $D(\psi)$, which depends on deformation and temperature through the bulk free energy density Δf and through the logarithmic term including the orientation distribution of single elements $w_{am}(\psi)$ (cf. eq V-15). In the equilibrium theory the sharpening results from (i) deformation-dependent equilibrium degree of crystallinity and number density of chains and (ii) "morphological transitions". The latter means that at high temperatures and large deformation most of the chains contribute fully extended "side-chain crystallites", while at low temperatures and/or small deformation ratios some chains are able to overcome the barrier of folding and form folded single-chain elements. In consequence, the sharp orientation distribution of extended chain crystallites is modified by the broad distribution of folded crystallites.

The calculated orientation distribution functions for the (110) and (020) reciprocal lattice vectors are presented in Figures 20a,b. The values of model parameters were chosen as follows: $A = 20$, $\delta = 90°$, and $\kappa_0 = 0°$ for the (110) plane or $\kappa_0 = 66°$ for the (020) plane. The equilibrium theory predictions were used for the c-axis distribution, $W_c(\psi)$. Although simulated distributions do not fit the experimental data well, qualitative features are satisfactorily reproduced.

In particular, the experimental data indicate that the maxima of the (110) vector distribution function are shifted with respect to $\psi = 90°$ by some 10–20°. Model calculations with arbitrarily chosen values of A, δ, κ_0 predict a similar shift, but smaller than the observed one (5–10°). The shift in the (110) distribution can be explained on the basis of nonuniform η angle distribution without any tilting of the c axis with respect to the lamellar basal plane (see Figure 15b). Existing experimental data are not sufficient to indicate which one of the two mechanisms (tilting of the c axis or crystallite anisotropy) is responsible for the observed phenomena.

Acknowledgment. We are grateful to Professor R. S. Stein for his valuable comments on our paper. We acknowledge financial support of the Ministry of Education, Science, and Culture, Japan, which provided Grants No. 449012 and 56490013 to T.H. and a scholarship in 1982/83 for M.K. We are grateful to the Japan Society for the Promotion of Science, which supported part of this work within the framework of the Polish–Japanese Scientific Cooperation and provided a visiting grant for A.W. in 1979. A.Z. acknowledges support from the Society of Fiber Science and Technology, Japan (Sen-I Gakkai), which made possible his stay in Kyoto University in 1981/82.

References and Notes

(1) Flory, P. J. *J. Chem. Phys.* **1947**, *15*, 397.
(2) Smith, K. J. *Polym. Eng. Sci.* **1976**, *16*, 168.
(3) Wu, W. L. *J. Polym. Sci.* **1978**, *16*, 1671.
(4) Krigbaum, W. R.; Roe, R. J. *J. Polym. Sci., Part A-2* **1964**, *2*, 4391.
(5) Gaylord, R. J. *J. Polym. Sci., Polym. Lett. Ed.* **1975**, *13*, 337; *J. Polym. Sci., Polym. Phys. Ed.* **1976**, *14*, 1827.
(6) Baranov, V. G.; Elyashevich, G. K. *Vysokomol. Soedin., Ser. B* **1974**, *16*, 611.
(7) Jarecki, L.; Ziabicki, A. *Polymer* **1978**, *20*, 411.
(8) Allegra, G. *Makromol. Chem.* **1980**, *181*, 1127.
(9) Gehman, S. D.; Field, J. E. *J. Appl. Phys.* **1939**, *10*, 564; *J. Appl. Phys.* **1944**, *15*, 371.
(10) Kawai, T.; Iguchi, M.; Tonami, H. *Kolloid Z.* **1968**, *221*, 28.
(11) Hill, M. J.; Keller, A. *J. Macromol. Sci., Part B* **1969**, *3*, 153.
(12) Lunch, D.; Yeh, G. S. Y. *J. Macromol. Sci., Part B* **1973**, *7*, 121.
(13) Cesari, M.; Perego, G.; Zazzetta, A.; Gargani, L. *Makromol. Chem.* **1980**, *181*, 1143.
(14) Krigbaum, W. R.; Balta, Y. I.; Via, G. H. *Polymer* **1966**, *7*, 61.
(15) Yeh, G. S. Y.; Geil, P. H. *J. Macromol. Sci., Part B* **1967**, *1*, 251.
(16) Krigbaum, W. R.; Maruno, S. *J. Polym. Sci., Part A-2* **1968**, *6*, 1733.
(17) Su, T. K.; Mark, J. E. *Macromolecules* **1977**, *10*, 120.
(18) Göritz, V. D.; Müller, F. H.; Sietz, W. *Colloid Polym. Sci.* **1974**, *252*, 330.
(19) Kobayashi, K.; Nagasawa, T. *J. Macromol. Sci., Part B* **1970**, *4*, 331.
(20) Hashimoto, T.; Ishido, S.; Kawai, H.; Ziabicki, A. *Macromolecules* **1978**, *11*, 1210.
(21) Kośc, M.; Ziabicki, A. *Macromolecules* **1982**, *15*, 1507.
(22) Chirico, A. D.; Lanzani, P. C.; Raggi, E.; Bruzzone, M. *Makromol. Chem.* **1974**, *175*, 2029.
(23) Bruzzone, M.; Mazzei, A.; Giuliani, G. *Rubber Chem. Technol.* **1974**, *47*, 1175.
(24) Bruzzone, M.; Sorta, E. *Polymer* **1978**, *19*, 467.
(25) Saijo, K.; Wasiak, A.; Hashimoto, T.; Kawai, H., to be submitted to *Macromolecules* (part 3 of this series).
(26) Saijo, K.; Ohta, Y.; Suehiro, S.; Kawai, H.; Hashimoto, T., to be submitted to *Polym. J.* (part 1 of this series).
(27) Fujimura, M.; Hashimoto, T.; Kawai, H., *Mem. Fac. Eng., Kyoto Univ.* **1981**, *43*, 224.
(28) Hashimoto, T.; Suehiro, S.; Shibayama, M.; Saijo, K.; Kawai, H. *Polym. J.* **1981**, *13*, 501.
(29) Stein, R. S. *J. Polym. Sci.* **1958**, *31*, 327.
(30) Wilchinsky, Z. W. *J. Appl. Phys.* **1959**, *30*, 792.
(31) Ziabicki, A. *J. Chem. Phys.* **1968**, *48*, 4368.
(32) Ziabicki, A. *J. Chem. Phys.* **1977**, *66*, 1638.
(33) Ziabicki, A.; Jarecki, L., IFTR Reports (Inst. Fundamental Technological Research, Polish Academy of Sciences, Warsaw, Poland), no. 1, 1982.
(34) Jarecki, L.; Ziabicki, A. *Polymer* **1977**, *18*, 1015.
(35) Ziabicki, A.; Jarecki, L. *Colloid Polym. Sci.* **1978**, *256*, 332.
(36) Jarecki, L.; Ziabicki, A. *Polymer* **1979**, *20*, 411.
(37) Roe, R. J.; Krigbaum, W. R. *J. Appl. Phys.* **1964**, *35*, 2215.
(38) Hoffman, J. D.; Davies, G. T.; Lauritzen, J., Jr. *Treatise Solid State Chem.* **1976**, *3*.
(39) Alexander, L. E. "X-ray Diffraction Methods in Polymer Science"; Wiley: New York, 1969; Chapter 4.
(40) See, for example: Guinier, A.; Fournet, G. "Small-Angle Scattering of X-rays"; Wiley: New York, 1955; Chapter 3.4.
(41) See, for example: Hosemann, R.; Bagchi, S. N. "Direct Analysis of Diffraction by Matter"; North-Holland Publishing Co.: Amsterdam, 1962.